D. B. Gadkari. International Journal of Engineering Research and Applications
www.ijera.com
ISSN: 2248-9622, Vol. 10, Issue 5, (Series-IV) May 2020, pp. 07-20

RESEARCH ARTICLE OPEN ACCESS

The homogeneous and entire detached $In_{0.5}Ga_{0.5}Sb$ alloy crystals grown by the slow freezing using novel VDS-process

D. B. Gadkari*
Freelance Research & Consultant; Crystal Growth and Technology
Embee-10A, Saibaba Nagar, Borivali (W), Mumbai-400092 India
Corresponding Author: D. B. Gadkari

ABSTRACT
First time, the homogeneous and the entire detached In0.5Ga0.5Sb crystals were grown using the step by step growth process by a vertical directional solidification process (VDS-process). The growth stability, crystal appearance, and growth habit of the In0.5Ga0.5Sb crystals were studied. The composition % 'x' changes showed the conversion n-type to p-type along c-axis. Novel In0.5Ga0.5Sb crystals were exhibited the electron mobility 1.59x104cm2/V.s in n-type region, and the hole mobility increased highest to 935cm2/V.s in p-type region. Indium segregations reduction showed the increased resistivity to 1.1 x10-3 Ω-cm, and decreased dislocation density to 103cm2. The tuned energy band gap 0.16eV to 0.68eV, and microhardness 2.19GPa to 3.98GPa was measured. The entire detached In0.5Ga0.5Sb crystals showed the preferential (022) growth. The axial and the transverse indium segregation was ~0.0802 mol% per mm. In0.5Ga0.5Sb crystal is advantageous, and encompass the electromagnetic spectrum for the infrared devices. The composition % and transport properties of In0.5Ga0.5Sb crystallization significantly enhanced, the causes are studied in this article.

Keywords: In0.5Ga0.5Sb Crystal, detached growth, Crystallization, Slow freezing, Physical properties

---

Date of Submission: 13-05-2020 Date of Acceptance: 26-05-2020

I. INTRODUCTION

InxGa1-xSb alloy crystal synthesis and crystallinity is a challenge [1-12], and challenges are: i) The binary InSb-GaSb phase with the temperature difference of liquidus-solidus phase is a problem. The pseudo-binary solid is composed of the InSb and GaSb melt. ii) A pseudo-binary phase of liquidus-solidus phase shows no congruent growth, iii) it causes heterogeneity and segregation component distribution. iv) $In_{0.5}Ga_{0.5}Sb$ crystal has intriguing physical and chemical properties. v) The obstructions are crystal structure defect, difficulty of the high mobility and the crystallography, the high lattice thermal conductivity. Crystals are viable materials for the next-generation sophisticated applications [2-12]. Potential applications are: LWIR: Thermoelectric (TE), high-speed electronic; MWIR: Photonic sensors, high speed devices; SWIR: MOS circuits, Optoelectronic, Solar cell; NIR: Light emitting diodes, TPV.

High-quality Ga0.86In0.14Sb ingots were grown suppressing segregation by VB method using the rotating magnetic field (RMF). The grown crystal mobility and resistivity were $1.618x10^3$ $cm^2/V{\cdot}sec$ and 1.162 $x10^{-3}$ Ω·cm, respectively [2]. The stoichiometric Nanowires (NWs), the $0.09<x<0.28$ with uniform phase-purity and the orientation were grown by Chemical Vapour Deposition (CVD). The In0.09Ga0.91Sb showed the high hole mobility 463cm2/V.sec [3**].** A ZT maximum, 0.57and 0.4 (at 780 K) were obtained for the In0.6Ga0.4Sb and In0.85Ga0.15Sb respectively by 'Ga' doping into InSb [4]. **C**rystal growth of the In0.11Ga0.89Sb (ISS) was grown at the space program SJ-10, in microgravity. The composition and uniformity were achieved with higher growth rate under microgravity [5]. The indium distribution in ternary Ga0.8In0.2Sb alloys doped ingots were grown by VB system [6]. III–V ternary InxGa1-xSb crystal's lattice constant can change with the composition % 'x' and modify the electrical properties and a band gap width. The Ga1-xInxSb compounds, the lattice parameter of the alloy can modify from 6.09 Å to 6.48 Å, and the band gap from 0.72 eV to 0.18 eV [7]. The growth process of InxGa1-xSb alloy crystals using sandwiched structure of GaSb (seed)/InSb/GaSb(feed) under normal and μG conditions were studied [8]. Comparative studies of the formation of impurity heterogeneity in crystals by the crystallization under space and ground conditions were reported [8]. The spreading resistance and the resistivity reveal heat and mass transfer. Axisymmetric heating by vertical furnace decreases 2–3 orders convections into melt, similar as in microgravity [9]. Influence of

microgravity on crystal growth in orbital spacecrafts were investigated, the experimental data of crystal growth in microgravity were analyzed [10]. The homogeneous growth of mixed material is a problem, increases change in properties by chemical composition. A challenge of the soluto-capillary convection in a melt was investigated [11].

Crystals at high temperature were grown to understand diffusion effects. Novel exciting way to measure the solid state diffusion in real time was the neutron imaging of vertical gradient freeze crystal growth [12].

High-order crystals were grown by the "Detached Phenomenon" using VDS-process, the homogeneous and chemically uniform structure of the grown crystals were studied [13-20]. The systematic study of the InxGa1-xSb (x=0.5) alloy crystals were evaluated by the quality and properties. In this research work, the entire detached six $In_{0.5}Ga_{0.5}Sb$ alloy and the homogeneous crystals were grown by the novel VDS-process underground condition to study the fundamental of crystal growth from a melt and the crystallization by slow freezing

.

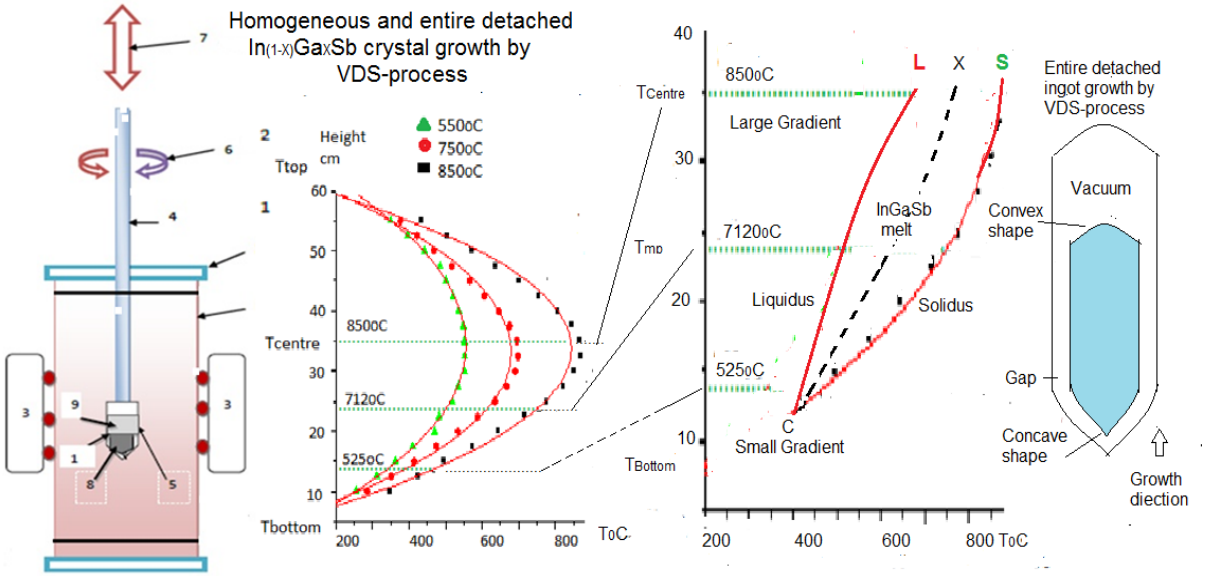

Figure- 1 The schematic diagram of the VDS process a) a quartz growth chamber, 2) Wilson seals, 3) a vertical furnace with the thermocouples (red circles), 4) a vertical shaft to hold the ampoule at the centre of furnace, 5) a vacuum sealed quartz ampoule, 6) the clockwise and anti-clockwise rotation 7) the up and down movement of an ampoule, 8) as grown detached ingot inside ampoule, 9) the vacuum (open space) above a melt, 10) the vacuum sealed quartz ampoule with source materials inside details, 11) The open quartz tube covered with the silicon wool, 12) The bottom Wilson seal is removed and exposed to ambient temperature. b) The temperature profile of furnace. The height of furnace was 66cm, the hot zone of furnace at the 33cm (center). c) The arrangement assist to control the phase change, heat transfer, fluid flow, solute transport, and segregation, thus single crystal growth of Sb-based crystals are promoted. In VDS-process, the radial gradients are 1.4^0C/cm and the axial gradient decreases towards lower temperature from large gradient condition (32^0C/cm) to small gradient condition (12^0C/cm). The large temperature gradient, the liquidus (L)-solidus (S) curves never comes closer; both are away from each other. The small temperature gradient zone the liquidus-solidus curve comes closer, it help for entire detached ingots growth. 'x', the homogeneous and uniform composition %. d) The schematic as grown entire detached crystal (light blue colour) with a gap between the inner ampoule wall and grown ingot. The convex, concave, vacuum is shown. The growth direction was against gravity (anti-gravitational solidification), while ampoule was translated down word in the gravity.

II. IEXPERIMENTAL PROCEDURE

2.1. Preparation of Six $In_{0.5}Ga_{0.5}Sb$ crystals

First time, the vertical furnace was designed for the crystal growth without a seed to study the crystallization from a melt by VDS-process underground condition [13-20]. The $In_{0.5}Ga_{0.5}Sb$ alloy crystals of high-purity were grown by VDS-process using the source materials In, Ga, Sb (5N, Alfa Aesar) in staichiometric proportion, Table-1. These materials were enclosed into the fused quartz ampoule, oxygen, nitrogen and impurity contaminations were minimized. The initial step was

to control the pressure of an inert argon gas, an ampoule by vacuum ~$1.3x10^{-3}$Pa, purged alternately for 10 times by back refilling high-purity an argon gas. An argon gas (0.027MPa) was sealed with a vacuum and source materials. Ampoule was positioned vertically in an exclusive arrangement of a vertical furnace. The ampoule with a tip angle (~450 to~750), the diameter 10-22mm and the.

Table-1 Staichiometric source materials for the growth of $In_{0.5}Ga_{0.5}Sb$ (IGS grms)

Sr No.	Elements	IGS-1	IGS-2	IGS-3	IGS-4	IGS-5	IGS-6
1	In	5.3955	5.1135	5.3703	4.1695	4.2204	4.8127
2	Ga	3.2929	3.1038	3.2977	2.5310	2.5629	2.9223
3	Sb	11.6100	10.9518	11.4135	8.8444	8.9576	10.2071
4	InGaSb	18.2984	19.2691	20.0815	15.5449	15.7509	17.9421

length 100mm were fabricated

2.2. $In_{0.5}Ga_{0.5}Sb$ crystal growth process

The furnace temperature profile to supply the heat, the growth conditions and parameters were fixed from previous VDS experiments (CGRP) [19]. The seven steps crystal growth process was i) The furnace temperature was raised in 3h to set temperature ~850^0C to melt In-Ga-Sb source materials in a zone $T_{centre}>T_{mp}> T_{bottom}$, Fig 1, then kept for mixing 3h for the congruent and the homogeneous melt of source materials. ii) The ampoule enclosed with source materials' melt, was translated downward by the lowering rate 10mm/h for 3h to the fixed set temperature ~765^0C growth, i.e. 50^0C above the melting point (m.p) of GaSb. The crystal-melt (C/M) interface was in the range of 712^0C to 525^0C (m.p. GaSb, InSb) into a zone $T_{mp}> T_{bottom}$ Fig-1. iii) The steady isotherm and steady thermal states were maintained for the homogeneous and chemically uniform melt for 3h. iv) The sensitive growth stage, an ampoule containing the homogeneous and congruent melt was translated downward from the set fixed temperature (~765^0C) by the slow freezing rate 1.38μm/s or ≤5μm/s (growth velocity 'v') in the vertical furnace. The gradients were the large axial (32^0C/cm) and small axial (12^0C/cm), while the low radial gradient was constant at 1.4^0C/cm. An ampoule was rotated at the 10 rpm clock-wise throughout the growth to achieve the homogeneous, uniform composition and temperature distribution into melt during growth. The measured growth period was ~ 4h, v) as grown ingot was lowered 10mm/h within 3h below 100^0C of the InSb m.p., kept at this temperature for thermal stabilization for 3h. vi) the furnace fixed set temperature (~7650C) was lowered to 2500C below the previous step temperature (~4250C), then switched off for a natural cooling for 3h, vii) the last step, switch-off the furnace, then wait for 2h to cool down the as grown In0.5Ga0.5Sb ingot. Finally, take out the grown ingot from the vertical furnace at room temperature (RT).

a b c d

Figure-2 the sequence of the taking out ingot from ampoule, the as grown detached ingot were grown by VDS-process, a) As grown entire detached Sb-based ingot, b) Ingot taking out from an ampoule, c) The empty ampoule, d) The grown ingot and its surface features.

Ingot growth period was ~26h; the total growth period was ~48h, as grown In0.5Ga0.5Sb ingots came out easily by the tapping an ampoule. The excessive heat of conduction was prevented by no

downward support to an ampoule. Ingot taking out process is in Fig-2. Six entire detached In0.5Ga0.5Sb ingots are shown in Fig-3. The substrate dimensions were - 10mmx10mmx0.3mm. A vertical furnace was controlled by PID, however, the quartz tube acts as a thermal seal.

2.3 The optimization of growth rate for Sb-based crystals

Growth of the Sb-based semiconductor is the thermodynamically process [20]. The m.p. of Sb-based materials were used to calculate the maximum set limit of the ampoule translation velocity 'v'. Calculated set limit of the crystallization velocity is 'v' from thermodynamically condition, the growth rate of Sb-based crystal requires 'v' <9cm/h. The crystallization velocity is proportional to the thermal diffusivity to conduct the thermal energy, i.e. the thermal conductivity of the quartz ampoule wall by thermal diffusivity. The temperature gradient in the furnace is imparted through the ampoule wall to the Sb-based material. Thermal diffusivity of the quartz is ≈ 0.010 cm^2/s, hence 'v' was select as ~ $1/10^{th}$ of the Sb-based materials. The maximum limit on the crystallization becomes: v < 9mm/h by slow freezing. Seventy-two crystals of the Sb-based materials [13-20] of the growth rates <7mm/h were grown. The selected velocity 'v' was ≤5mm/h (≤1.38 µm/s) for $In_{0.5}Ga_{0.5}Sb$ crystallization.

Figure-3 The as grown ingots of $In_{0.5}Ga_{0.5}Sb$, a) IGS-1, b) IGS-2, c) IGS-3, d) IGS-4, e) IGS-5, f) IGS-6

2.4 Equipment's used for characterizations

$In_{0.5}Ga_{0.5}Sb$ grown ingot was sliced longitudinal and transverse to the preferentially grown (022) direction, to use for the measurements and characterizations at RT. The substrate thickness was <500µm by Buchler ISOMAT Low speed saw and diamond cutter using Low Speed Saw and Metacut-DC-I. The substrate dimensions were 10mmx10mmx0.3mm, the substrate was prepared by the cleaning, grinding, lapping by carborrundum power (0.5µm), and polishing to mirror finish by 0.1 and 0.03µm alumina abrasive powder by Metapol DC-II. Growth morphology was developed by selective chemical etching CP4, and modified CP4. The microstructures were characterized by the Scanning electron microscopy SEM (JEOL JSM-840). Composition % analysis was determined by EDAX (Analer Kevex). The crystal dislocation

density (dd) were measured using Metallurgical microscope (Carl Zeiss, Karl Suss MJB-3, Metagraph-I Metatake), and Interface contrast microscopy Nomarsky (Leitz Arisomet vaviport wild 46). Ingots crystallinity and crystallization were characterized by X-ray diffraction, the phase structures were investigated by X-ray diffraction (JEOL JDX8030, SIEMENS Krystalloflex diffractometer) using CuKα radiation, λ=1.504A^o. Laue spectrometer (Huber) was used for the single crystal growth and orientation analysis. Hall measurement along the radial and axial direction was measured by Four probe CTI closed cycle Liquid helium crystal model No M22 with Keithley-220-current sources and 182-nonovoltmeter. Raman spectroscopy, the lattice vibration and excitations was measured by PerkinElemer-2000. Energy gap was measured by FTIR (Perkin-Elmer-GX), Spectrum-65, Biorad-45. Infrared characterization by ISS 88. The hardness was measured by Vickers micro-hardness test (MVH-I Metatak). These could facilitate to confirm Novel VDS-process.

Table-2

Ele	IGS-1		IGS-2		IGS-3		IGS-4		IGS-5	
	Wt%	At%	Wt%	At%	Wt%	At%	Wt%	At%	Wt%	At%
In	18.13	14.57	18.72	17.10	17.80	17.92	18.42	16.86	17.42	15.86
Ga	30.70	44.39	29.26	40.36	28.66	38.66	29.42	40.61	29.42	41.61
Sb	51.17	41.04	52.02	42.54	53.54	43.42	52.06	42.52	52.06	42.52

a) The composition %, the Wt % of IGS6 is In=17.61%, Ga=29.42%, Sb=52.82%.

Elemen Wt gm	IGS-1		IGS-2		IGS-3		IGS-4	
	Actual Wt	Compo %	Actual Wt	Compo %	Actual Wt	Compo %	Actual Wt	Compo %
In	5.396	18.13	5.114	18.72	5.370	17.80	4.170	18.42
Ga	3.293	30.70	3.104	29.26	3.298	28.66	2.531	29.42
Sb	11.610	51.17	10.952	52.02	11.414	53.54	8.844	52.06
IGS	18.298		19.269		20.082		15.545	

b) Weight of elements and weight of elements calculated from the substrate composition %. EDAX Measurements: the composition % of the $In_{0.5}Ga_{0.5}Sb$ samples were selected from above the central part of the each ingot from the four detached crystals. A composition (%) measured after the conical shape (15mm) and before the convex shape (10mm), i.e. ~15-75mm.

III. RESULTS

3.1 Crystal Growth Research Projects (CGRP)

Crystal Growth Research Projects (CGRP), the three CGRPs have been completed. CGRP-I and II was focused on properties of the entire detached Sb-based crystals by VDS-process [19]. CGRP-III was focused on the fundamental of crystal growth from melt, and the crystallization from solution (melt) to understand the Science behind the entire detached growth. $In_{0.5}Ga_{0.5}Sb$ growth experiments were focused to reduce complex convective flows.

3.2 In0.5Ga0.5Sb crystal growth

The outer quartz tubes acts as a thermal seal for growing ingot (growth chamber), L=100cm and d=10cm was fixed at the centre of furnace (H=66cm) Fig-1. An equal length 17cm, above and below a black line of vertical furnace was exposed to RT. Furnace was designed for the pseudo binary phase growth of the entire detached bulk crystals. An open quartz tube length 17cm (T_{top}) was covered by the silicon wool to prevent heat radiation. Wilson seal at bottom was removed to expose growth chamber to RT. This provides the temperature difference > ~100^{0}C, Fig-1a. The ampoule was smoothly translated downward from the large axial gradients (32^{0}C/cm) to keep apart the liquidus-solidus curve to control homogeneous $In_{0.5}Ga_{0.5}Sb$ melt. The small radial temperature gradients condition was 1.4^{0}C/cm. Crystallization (solidification) by slow freezing of the melt at point 'C', where the small axial gradients (12^{0}C/cm), and the liquidus-solidus curve (L, S) congregate, Fig-1c,d. The conical end of a vacuum sealed ampoule was positioned at C/M interface above the GaSb m.p. Ingot solidification point 'C' acts as a seed, changes upward from 525^{0}C to 712^{0}C by increasing the composition % 'x' at the fixed set temperature ~760^{0}C (anti-gravitational solidification). The ingot crystallization rate at C/M interface was 0.69μm/s. whereas, the ampoule translation velocity 'v' was 1.39μm/s for the other steps. $In_{0.5}Ga_{0.5}Sb$ six crystals were grown - diameters (dia=10 to 22mm) and lengths (65 to 85mm). Detached ingot taking out process is shown in Fig-2, and the six as grown entire detached ingots are in Fig-3.

As grown ingots features are in Fig-3 - i) the entire detached crystals showed no micro cracks,

no ampoule cracks, no defects, no striations by the crystallization due to the reduced constitutional supercooling and indium segregation, ii) the ingots showed concave shape in beginning and iii) the convex shape of ingot at the end growth as the aspect ratio decreases, iv) the ingots showed the smooth shiny surface as surface energy was steady, v) a solid drop on the few ingots' top Fig-3d,e,f, was grown as the melt concentration difference decreasing along c-axis. The meniscus and C/M interface shape was convex (seen from a vacuum). Ingot end growth, a plane interface converts into two shapes - i) the stoichiometric In-Ga-Sb grow by a convex cap (hemispheric) at the ingot end Fig-3a,b,c, ii) the excess binary phase difference grow as a solid drop of GaSb on ingots end due to the concentration phase difference of binary and ternary melt, Fig-3d,e,f. The soluto-capillary convections were suppressed, it attributed the ingot homogeneous, uniform field and concentration distribution

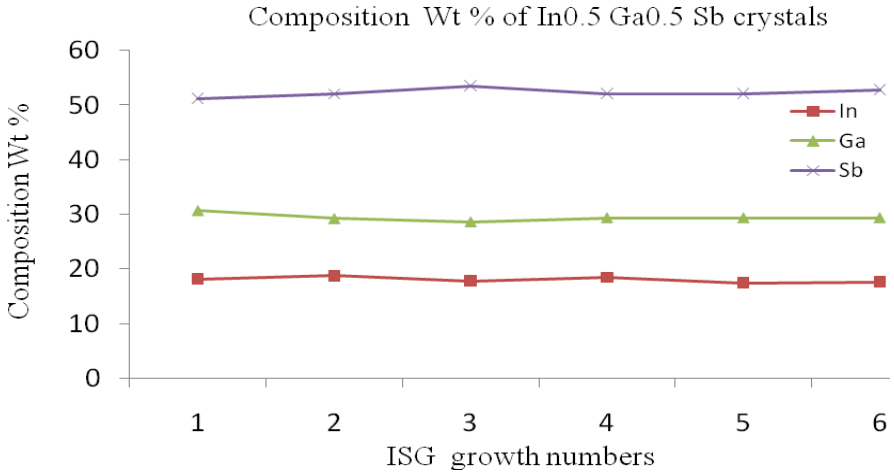

Figure-4 The graph of as grown IGS numbers versus the composition % of six $In_{0.5}Ga_{0.5}Sb$

3.3 Principle of the homogeneous and detached growth

The pseudo-binary InSb-GaSb crystals growth, the thermodynamically degree of freedom is one. Only the set temperature parameter is constant for the composition of the InSb-GaSb pseudo-binary melt. In the ternary $In_{0.5}Ga_{0.5}Sb$, the thermodynamically degree of freedom is two. One additional parameter is required to the set temperature, Fig-1b. The $In_{0.5}Ga_{0.5}Sb$ pseudo phase growth is shown in Fig-1c. Set temperature and curves of the L (liquidus), S (solidius) were two parameters, which were constant during growth. Whereas, the composition % 'x' was not constant, it increases along c-axix. Effective InSb-GaSb composition % was increasing along c-axis, schematically in Fig-1c. The ternary phase of $In_{0.5}Ga_{0.5}Sb$ increases from m.p.-525^0C (InSb) to 712^0C (GaSb). The curves L, S corresponds to the liquidus isotherm and the solidus iso-concentration curve respectively. The 'C' is an iso-point of the crystallization / solidification (acts as a seed) on the isotherm line of m.p. InSb to GaSb. The 'x' mole per mm composition % as well as crystallization moves from 525^0C to 712^0C at point 'C' in equilibrium state. Hence, the composition % 'x' increases from 00% to 100%, along c-axis (anti-gravitational solidification). Ampoule was moved downward velocity 'v' into the growth chamber. The pseudo phase converts into apparent controlled ternary solid at 'C', moves upward. Ingot detaches by the cohesive and surface energy by a vacuum and slow freezing. This is the principle of homogeneous and entire detached growth.

3.4 The composition % by EDAX

The composition % of four entire detached ingots by the EDAX showed in Fig-4. The substrates were selected from the middle part of as grown ingots to study changes in composition % 'x'. IGS-1, 2, 3, 4, the axial and transverse indium mol% per mm were 0.083, 0.0797, 0.0829, 0.0758. Actual weights of source materials (Wtgms) and composition % were used to calculate the target alloy crystals, Table-2a,b. Ingots composition: i) In0.04Ga0.96Sb ii) In0.07Ga0.93Sb, iii) In0.04Ga0.96Sb, and iv) In0.03Ga0.97Sb respective ingots in Table-2b, belong to p-type region of $In_{0.5}Ga_{0.5}Sb$ ingots. The hole motilities are in Table-4. Highest hole motilities ~935cm^2/V.sec, ~716cm^2/V.sec, ~1021cm^2/V.sec, ~1083cm^2/V.sec respective ingots. The crystallization state exist by the uniform diffusion an layer by layer growths at the axisymmetric temperature in a vertical furnace of

VDS-process. The fluctuations were decreased as melt solidify by slow freezing at C/M interface in a vacuum sealed ampoule. The crystallization, high-density, the uniform phase purity, and orientation were confirmed.

Table-3 XRD measurements of $In_{0.5}Ga_{0..5}Sb$, the substrates are selected from body of Ingots.

IGS1-12		IGS2-13		IGS3-11		IGS4-11		IGS5-10		IGS6-11	
2θ	d	2θ	d	2θ	d	2θ	d	2θ	d	2θ	d
24.27	3.705	25.289	3.520	25.18	3.534	23.76	3.742	24.96	3.564	24.12	3.705
39.70	***2.228***	***41.66***	***2.146***	***38.90***	***2.234***	***39.36***	***2.287***	***41.52***	***2.139***	***39.7***	***2.227***
46.90	1.936	49.55	1.838	41.46	2.176	46.50	1.951	41.62	2.168	46.9	1.936
57.14	1.64	60.72	1.524	49.32	1.846	71.32	1.321	49.22	1.85	57.14	1.64
62.84	1.478	66.81	1.399	60.42	1.531	71.68	1.316	49.40	1.84	62.84	1.478
63.08	1.477	76.51	1.244	66.52	1.404	76.40	1.246	60.28	1.534	63.08	1.477
71.72	1.315			76.06	1.25			65.72	1.42	71.72	1.315
76.94	1.238							75.74	1.255	76.94	1.238

The black numbers indicate the preferred (220) ingots growth direction, and the maximum I/I0 peak intensity ratio. The sharp peaks values for (220) diffraction, the ASTM/ JCPDS, CuKα λ=1.5405 A^0 i) card number 6-208 InSb: a=6.4782A^0, d=2.290, hkl=220, 2θ=39.9098, ii) card number 7-215 GaSb: d=2.156, hkl= 220, 2θ=41.8639

3.5 XRD measurements

The powder diffraction patterns of the six $In_{0.5}Ga_{0.5}Sb$ ingots by XRD were indexed to know crystal planes, were compared with standard ASTM / JCPDS card No. 6-208 (InSb) and No. 07-0215 (GaSb). A new peak position was appeared highlighted in black numbers, Table-3. The 2θ of peaks were slightly blue-shift toward the lower angle due to the larger ion radius of 'In'. The 'Ga' was in small composition % (GaSb) in beginning growth, except IGS-2 and IGS-5. These two growths, the 2θ of the peaks were slightly red-shift toward higher angle due to the large number of 'GaSb % increasing with increase composition %. The XRD peaks shift by composition % could be associated with phase transformation and orientation of the atoms. From composition %, The successfully incorporation of 'Ga' into the lattice of $In_{0.5}Ga_{0.5}Sb$ crystal was confirmed. The sharp peak of crystals showed well-crystallization. The entire detached six ingots reveal that the XRD patterns of the ingots' main diffraction peaks showed similarity, representing the zinc blende structure of ternary $In_{0.5}Ga_{0.5}Sb$. The preferential sharp peak (022) was within the data of aforesaid card numbers. Whereas, the crystal diffraction angle decreased with the decreasing 'd' value and FWHM due to high-order crystals by crystallization using VDS-process (vacuum). $In_{0.5}Ga_{0.5}Sb$ crystals were perfect crystals with the FWHM 123 to 157arcsec. InSb and GaSb growths were perfect single crystals and FWHM 48-86 arcsec, showed zinc blend crystal structures. Dislocations density, the structural defect and the ions present in the lattice increases FWHM of peak by reducing its peak intensity. XRD analysis was based on the Bragg diffraction equation nλ=2dsinθ.

3.6 Hall electrical measurement

The electrical properties of the six $In_{0.5}Ga_{0.5}Sb$ ingots measured by the Hall-van der Pauw method at 300K. Crystal quality was determined by the Hall parameters: the mobility (μ), the resistivity (ρ), the carrier concentration (n) and the Hall coefficient (R_H), Table-4 and Fig-5. Calculated by equation- [2]: i) The carrier concentration $n=1/R_He$, ii) The resistivity $\rho = VatD/I\ L$, iii) The mobility $\mu_H = R_H\sigma. = R_H/\rho$. Where R_H: Hall coefficient, V_a: the applied potential, I: the current, and the substrates

dimensions, t: thickness, D: width, and L: length The changes in composition % 'x' and electrical properties showed the conversion from n-type (InSb) to p-type (GaSb) along c-axis.

Table-4 Hall-van der Pauw measurements of the $In_{0.5}Ga_{0.5}Sb$ grown crystals

Sample numbers	Mobility(μ) $cm^2/V.s$	Resistivity(ρ) Ω-cm	Carrier Con (η) cm^{-3}	R_H Hall Coeff cm^3/Coloumb
IGS1-2	15923	$6.3x10^{-3}$	$2.54\ x10^{16}$	-100.1
IGS1-6	10110	$8.7\ x10^{-3}$	$7.13\ x10^{16}$	-87.9
IGS1-9	3282	$2.5\ x10^{-3}$	$2.54\ x10^{16}$	-8.21
IGS1-12	65.7	$2.1\ x10^{-3}$	$4.56\ x10^{16}$	+0.14
IGS1-16	935	$7.78x10^{-3}$	7.8910^{17}	+7.24

IGS3-2	12410	$2.98x10^{-4}$	$1.69x10^{18}$	-37.1
IGS3-5	9566	$5.14x10^{-4}$	$1.27x10^{18}$	-5.1
IGS3-8	6239	$6.98x10^{-4}$	$1.44x10^{18}$	-4.3
IGS3-11	3270	$3.16x10^{-4}$	$6.05x10^{18}$	-1.03
IGS3-14	716	$1.5x10^{-4}$	$9.51x10^{17}$	+1.07
IGS5-5	4128	$6.34x10^{-3}$	$1.13x10^{18}$	-26.34
IGS5-7	2489	$5.2\ x10^{-3}$	$9.3\ x10^{17}$	-12.94
IGS5-11	925	$7.78x10^{-3}$	$8.68x10^{17}$	+7.21
IGS5-16	1021	$9.1\ x10^{-3}$	$6.93\ x10^{17}$	+7.29
IGS6-3	2481	$1.1\ x10^{-3}$	$2.25\ x10^{18}$	-2.73
IGS6-5	2378	$6.7\ x10^{-4}$	$4.26\ x10^{18}$	-1.59
IGS6-11	1083	$3.18\ x10^{-3}$	$8.1\ x10^{17}$	+3.43

Crystal growth valid points i) n-type to p-type changes as the charge carriers from GaSb (isovalent 'Ga' acceptor state) increases and InSb (isovalent 'In' acceptor state) decreases. ii) the typical $In_{0.5}Ga_{0.5}Sb$-1, the electron mobility of InSb ($\mu=6x10^4cm^2/V.sec$) in n-type region decreases from $1.59x10^4cm^2/V.sec$ to $3282cm^2/V.sec$ along growth axis, because more and more 'Ga' acceptors' (GaSb %) were incorporating into ternary In-Ga-Sb chain. Whereas, in p-type region, the hole mobility increases from $\mu=67.5x10^3cm^2/V.sec$ to $935cm^2/V.sec$, GaSb ($\mu=1.2x10^3cm^2/V.sec$), because 'In' acceptors' decreases into ternary In-Ga-Sb chain. iii) the resistivity decreases to $1.1x10^{-3}\Omega.cm$. iv) the increased mobility and decreased resistivity showed the ternary $In_{0.5}Ga_{0.5}Sb$ ingot was well crystallized. Similar discussion was for other five ternary $In_{0.5}Ga_{0.5}Sb$ ingots, Table-4. The charge carriers showed high-order of crystal quality of the entire detached growths due to the compensation or passivation. Crystallization by the heat and mass transfer at C/M interface of the six ternary

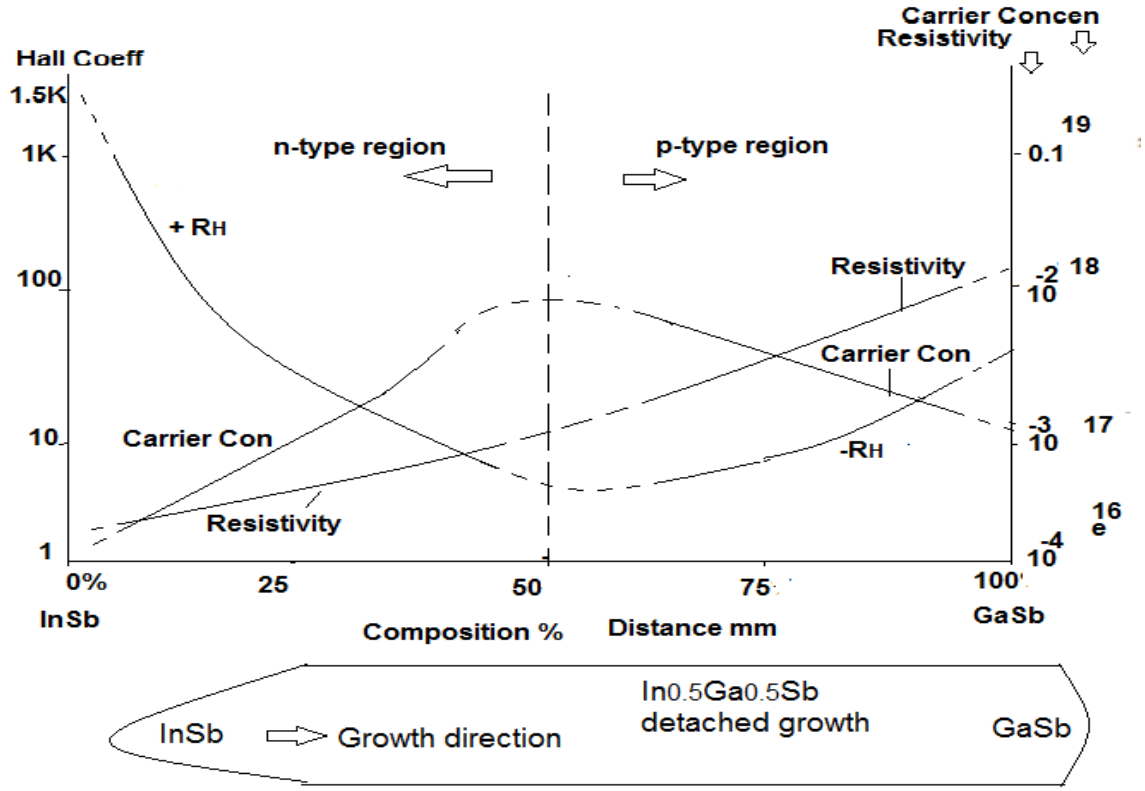

b

Figure-5 Hall-van der Pauw measurement a) the mobility and energy gap versus compositional %, b) the resistivity, the carrier concentration, and R_H versus the compositional %.

In0.5Ga0.5Sb alloy bulk crystals were confirmed. The energy band gap engineering: The mobility 'μ' decreases and energy Eg' increases in n-type region, whereas, the 'μ' and 'Eg' both increase, then

decreases in p-type region w.r.t. increasing composition % 'x', Fig-5. Notwithstanding, the small shift in the donor–acceptor ratio by the donor (Nd) and the acceptor (Na) concentrations (near to intrinsic) provides large fluctuations of 'ρ'. The acceptor acts as the p-type conduction for the concentration *N*a~10^{17}cm^{-3} (GaSb), whereas the donor *Nd* (InSb) concentration converts to the acceptor *(Na)*. The drift in 'ρ' establishes transition of the p-type conductivity. The ratio of donor-acceptor concentrations is very sensitive nearer to 50% composition. Because, the small changes of ratio (near intrinsic concentration) affecting 'ρ' variation. The lower 'ρ' and higher 'μ' values showed n-type conductivity *(Nd>Na).* Crystal growths of $In_{0.5}Ga_{0.5}Sb$ showed decreased dislocation density to 10^3cm^2, FWHM was 123 to 157arcsec.Reveals the evidence of lattice perfection of $In_{0.5}Ga_{0.5}Sb$ detached growths by VDS-process. The n-type crystals better electrical and optoelectronics properties showed in Table-4.

Macro and microscopic coefficients of heterogeneity was a ratio M= ($\Delta\rho/\rho$ x100%) [10], the Δρ was the mean square deviation and 'ρ' was mean value. Micro-uniformity was higher for detached $In_{0.5}Ga_{0.5}Sb$ crystals, fulfils required conditions for crystallization [20].

3.7 Effect of composition% 'x' on energy gap 'Eg'

The mobility (μ) and energy gap ('E_g) were measured by a Hall-van der Pauw method at 300K, showed in Fig-5, Table-5. The entire detached $In_{0.5}Ga_{0.5}Sb$ crystals have the complex properties nature. The electron mobility decreases up to composition 50% in n-type region, whereas the hole mobility of increases in p-type region. Hence, 'E_g' showed complex physical properties. Therefore, the effective acceptor concentration increases with the increase in 'Eg' IN N-TYPE-REGION; THE band gap energy increases from 0.16eV (InSb) up to <75%. Effective charge density state of an acceptor increases, thus Fermi level shifts below the valence band energy level (Eg). However, 'InSb' composition % further decreases, though the GaSb composition % 'x' increases. Fermi level shifts further below the band gap energy level EObs (maximum shift) by filling effective acceptor charge carriers.

Table-5 IR-measurements of $In_{0.5}$ $Ga_{0.5}$ Sb-1 crystals (IGS-1)

Sr No.	Sample No.	Wave number	Wavelength (μm)	Energy Gap (E_g eV)	IR range Application
1	InSb	1391	7.75μm	0.16eV	LWIR ~7-14 μm
2	IGS1-2	1427	7.0077	0.1769	
3	IGS1-4	1507	6.6357	0.1862	
4	IGS1-5	1521	6.5746	0.1886	
5	IGS1-6	1545	6.4725	0.1916	MWIR ~3-6 μm
6	IGS1-8	1663	6.0132	0.2062	
7	IGS1-10	1695	5.8997	0.2102	
8	IGS1-11	2042	4.8972	0.2532	
9	IGS1-13	2389	4.1684	0.2974	
10	IGS1-15	2736	3.6550	0.3393	
11	IGS1-18	3447	2.9010	0.4274	SWIR ~1-3μm NIR 0 .75-1 μm
12	IGS1-20	3815	2.6210	0.4731	
13	IGS1-22	4707	2.1243	0.5837	
14	GaSb	5208	1.7684	0.7012	

A transition from E_{Obs} to the conduction band energy level required large energy (Eg< E_{obs}), E_g = E_{Obs} - (E_U - E_{BM}). The shift is inversely proportional to effective mass by Burstein-Mass equation (BM). Log of alpha v/s energy, the reciprocal of the slope is Urbach Energy $\ln(\alpha) = \ln(\alpha_0) - \left[\frac{E_g - E_0}{E_U}\right]$,

In p-type region, 'E_g' decreases with increasing composition % (GaSb) >75% Table-5, Fig-5, with continuous in p-type region. The previous effective acceptor's charge density state (E_{Obs}) begins to reverse. Effective acceptor charge density (InSb) was further decreases, then Fermi level reaches the valence band energy gap (Eg). The effective concentration of the acceptors decreases (InSb% decrease), in contrast >75% (GaSb% increase) thus the accepters increase with increase in composition % 'x'. The effective band gap energy further decreases from its valence band gap energy level 'Eg'. Further decrease in indium, it acts the dopant (acceptor). Moreover, it occupies the shallow state above the valence band gap of $In_{0.5}Ga_{0.5}Sb$ (E_{Obs}), was < 0.68eV band gap energy of GaSb, Fig-5. Allowed shallow state occupy above the valence band gap by acceptors (indium), Fermi level shifts

up. The transition from energy level (E_{Obs}) to conduction band energy level requires low energy ($E_{Obs} < E_g$). The effective charge states follow the Urbach tail (E_U) and Burstein-Mass (E_{BM}). $E_g = E_{Obs} + E_U - E_{BM}$..

Resistivity increases with increasing in composition %, the carrier concentration increases up to <75% in n-type, then decreases after >75% in p-type region Fig-5b. Hall coefficient was decreased in n-type region and increased in p-type region. The conversion attributed to the high-crystalline quality of entire detached ternary In0.5Ga0.5Sb alloy crystal.

3.8 Raman spectroscopy

In0.5Ga0.5Sb substrate, Raman spectra of substrate from the n-type region of the In0.5Ga0.5Sb-1 is shown in Fig-6a The prominent sharp peak at 181.7cm-1 was υTO (Γ) modes and the low peak at 192cm-1 was υLO (Γ) modes showed two dominant peaks of the transverse optical (TO) and longitudinal optical (LO).

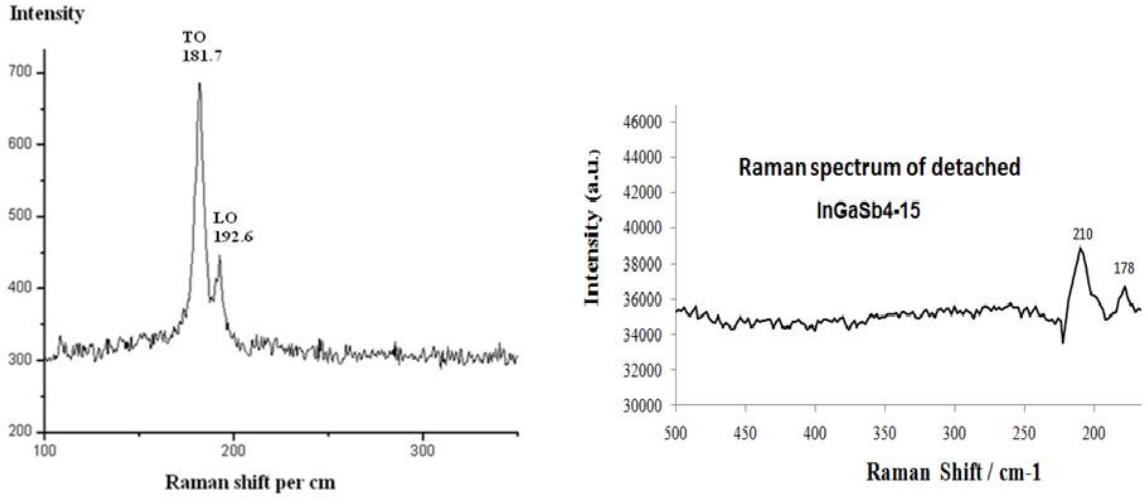

Figure-6 Raman spectra, a) the growth number IGS1, b) the growth number IGS4

Similarly, A substrate from the p-type region of the $In_{0.5}Ga_{0.5}Sb$-4 spectra is shown in Fig-6b. The prominent sharp peak at 210 cm^{-1} was υTO (Γ) modes, and the low peak at 178 cm^{-1} was υLO (Γ) modes. First vibration mode of sharp peak showed the crystallization direction of the ingots and the second peak showed the defect density. These peaks showed the reduced defect and the lower dislocation density. $In_{0.5}Ga_{0.5}Sb$ ingots lattice vibration and interaction with the excitations were studied by Raman spectroscopy. Raman shift was interaction between bonds of similar energies in a molecule, lead to a spectrum shift different by molecules vibrations. Raman spectra of binary GaSb and InSb showed the sharp peak at 221.65cm^{-1} and 174.2 cm^{-1} respectively, was identified as υTO (Γ) modes and the anti-stokes zinblende structure. Only TO phonon showed the (011) backscattering direction. It shows the single orientation growth. The perfect crystals growths of the $In_{0.5}Ga_{0.5}Sb$ crystals by VDS-process were confirmed.

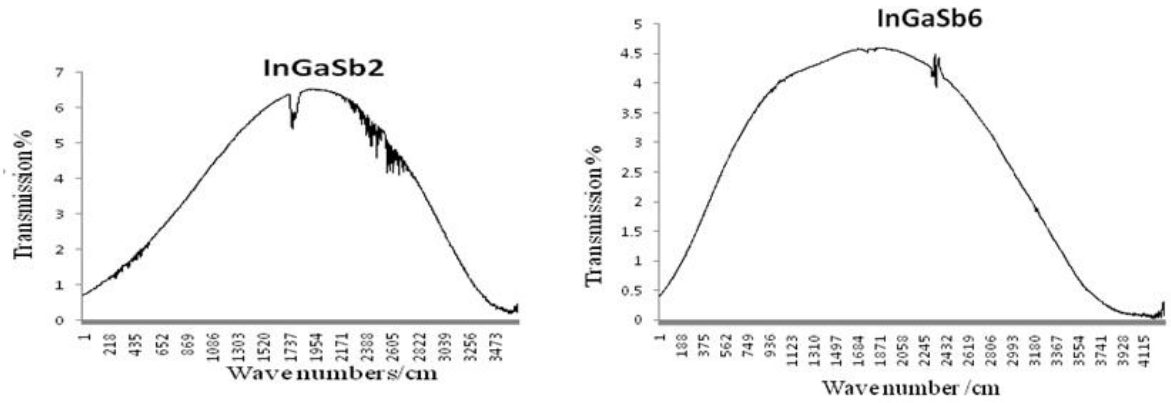

Figure-7 FTIR a) growth number IGS-2, b) growth number IGS-6

3.9 FTIR measurements

The band gap engineering and the wavelength along c-axis showed as the function of composition % 'x'. Energy band gap of $In_{0.5}Ga_{0.5}Sb$-1, and 4, the Eg=0.37eV (wave number 2965/cm), and Eg=0.38eV (wave number 3097/cm) repectively. FTIR graphs showed in Fig-7, and the fall in transmission of the band edge absorption and the dropping of transmission faster by the free carrier absorption. IR-measurements of the detached $In_{0.5}Ga_{0.5}Sb$-1 ingot showed in Table-5, the energy of gap E_g modified from 0.1769eV to 0.5837eV for range 8-2µm (wavelengths). Engineering of energy band gap, the composition % changes depends on the lattice constant; the ternary $In_{0.5}Ga_{0.5}Sb$ crystal's lattice constant was altered by the composition % 'x, the electrical properties in Table-4. the band gap width was also modified. IR-measurements of $In_{0.5}Ga_{0.5}Sb$-1 growth showed in Table-5, attribute entire detached growths were perfect crystals of InSb, $In_{0.5}Ga_{0.5}Sb$ and GaSb covers the IR-spectrum for device applications. The binary detached ingot's energy gap, InSb $E_{g\ was}$ 0.16eV, InSb:Bi Eg=0.15eV for the wavelength 7.75µm and 8.27µm respectively. GaSb E_g was 0.68eV and GaSb:Se E_g=0.78eV for the wavelength 1.92µm, and 1.58µm respectively. Transmission of the FTIR was 38% for InSb and 34% for GaSb, it showed perfect single crystals growth. The ternary $In_{0.5}Ga_{0.5}Sb$ detached ingots showed the low FTIR transmission as compared to binary entire detached crystals. The n-type region: The engineering of the band gap varies and potential for LWIR from 0.15eV to 0.21eV. The p-type region: The band gap varies and potential for SWIR from 0.3eV to 0.58eV. Between these two bands, the band gap varies and potential for MWIR 0.2eV to 0.3eV. Table-5, Infrared band ranges for electromagnetic spectrum, LWIR-8-12µm, MWIR-3-6um, SWIR- 1-2.5µm and NIR-0.75-1µm.

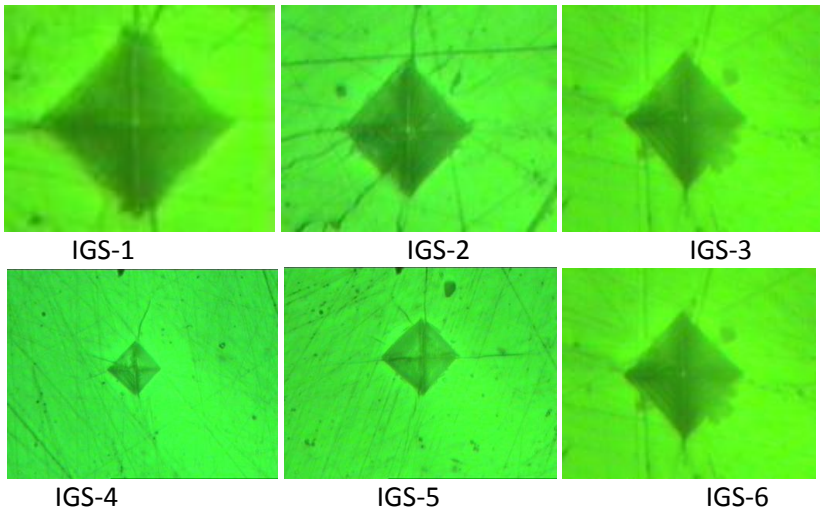

Figure-8 Microhardnes, the indentations of six $In_{0.5}Ga_{0.5}Sb$ crystals

3.10 Micro-hardness measurements

Vickers microhardness test by indentations method, the resistance force of bond could be known from the energy gap Eg and the hardness of covalent crystals. Hardness of covalent crystals was given by $Hv = CNeEg = CEg\ (Ne / 2)^{2/3}$ where C: constant of proportionality, Eg: Energy gap, Ne: electron density. The indentations of the six $In_{0.5}Ga_{0.5}Sb$ crystals showed in Fig-8. Microhardness of samples were IGS1=2.19GPa, IGS2 = 2.87GPa, IGS3 =3.02GPa, IGS4 = 3.72GPa, IGS5= 3.85GPa, IGS6 =3.98 GPa. Binary InSb and GaSb Hv = 2.21GPa and Hv= 4.42 GPa respectively. The higher value of hardness (Hv) reveals the higher crystalline growth. The higher hardness's attributed to the lower dislocation density and perfection in crystals, however, dislocation density (dd) relates to the hardness. First case was the extremely high order strength for the $dd<10^3cm^{2,}$ for the perfect single crystals. The dislocation motion was due to the breaking of covalent bonds of atoms, thus hardness increase with more breaking of the covalent bonds. Second case was perfect crystal, the range 10^3cm^2 to 10^4cm^2 hardness increase by dislocation-dislocation motion. Third case, dd $>10^4cm^2$, the hardness decreases with increase in dd by the motion of dislocations energy.

3.11 Growth morphology of In0.5Ga0.5Sb

Six $In_{0.5}Ga_{0.5}Sb$ ingots showed completely different growth morphology features Fig-9. The curved microstructures away from the edge of substrate due to the melt flows, the thermo-capillary

and thermo-capillarity concentration convection by the soluto-capillary, heat and mass transfer Fig-9-aI. Thermal mechanism process was tangential through the meniscus curve directed towards C/M interface. The featureless surfaces confirm the controlled convection of the concentration near interface front, Fig-9aII, III. The impurity black bands at the centre of substrate continues throughout with the uniform shape vertically, Fig.9-aIV. The morphology of microscopic growth was slow freezing at atomic level, ensures the solute, heat and mass transfer condition only by diffusion. Dislocation density decreased to $10^3 cm^2$ with the increased hardness; it reveals the higher order of crystals crystallinity. The perfect crystal (mass block) related to the entire detached In0.5Ga0.5Sb alloy growth properties, was totally confirmed. The dd > 104cm2, the quality deteriorate with the increases dd for worst crystal. A coherent twin boundary was the high degree of crystal perfection Fig-9b. The oriented two grains were together at the boundary plane. Low angle twin boundary (angle <150) was a plane mirror images, thus a twinned crystal was single plane of atoms.

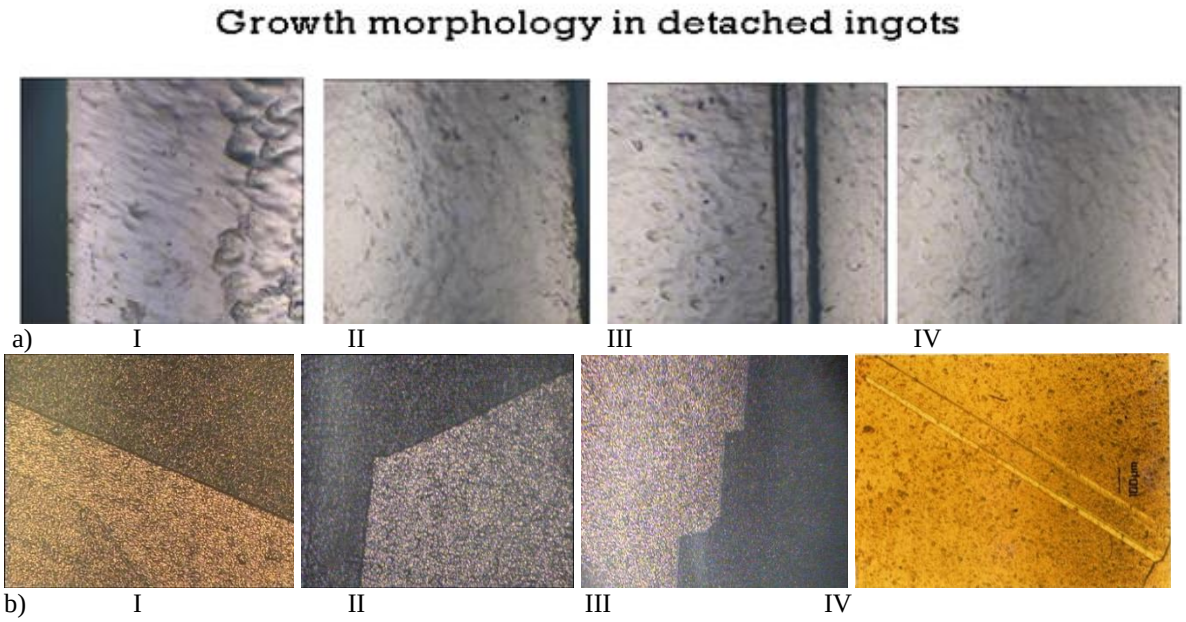

Figure-9 a) I) The curve micro growth away from the edge of substrate, II) The plane growth at the middle region of the ingot, III) The antimony black bands at the centre of the ingot, and IV) The plane growth above the middle region of the ingot. b) I) A low energy plane a plane for a twin boundary. II- III) Energy optimization by faceting on a plane The total area increases, but the energy decreases, IV- Twin lamella on low energy plane

The coherent twin boundaries were the crystals' internal structure formed by a mirror image itself along the shared border. Twin boundaries were occurred for the two crystals having similar nature of intergrowth. Highly symmetric interface with one crystal was other the mirror image. The atoms could share the two crystals at regular intervals with lower interface energy Fig-9b. The shape of the C/M interface during crystal growth was not flat or slightly convex, then resulted in large thermal stresses in crystals. It resulted in increased dislocation density and the number of defects such as twins, grain boundaries and microcracks.

3.12 The convections reduction into melt

Uniform composition distribution by complex flows need minimum thermal kinetic by the concentration convection and the temperature convection into melt are given below.

$$Ma_c = \frac{\left(-\frac{\partial \gamma}{\partial c}\right)H}{\mu D} \Delta c, \quad and \quad Ma_T = \frac{\left(-\frac{\partial \gamma}{\partial T}\right)H}{\mu D_T} \Delta T$$

Former equation is the Marangoni's thermo-capillary concentration convection and the later equation is the Marangony's thermo-capillary temperature convection. These convections' influence the optimum non-steady state into melt in a vacuum sealed ampoule. The strong buoyant thermo gravitational convection (steady state) influences the transportation, and then increases the segregation, interface fluctuation and the breakdown of C/M interface. It was reduced sufficiently in a vacuum sealed ampoule using VDS-process. Detached phenomenon is an excellent condition for the crystallization by slow freezing in vertical furnace. Whereas, the thermo-capillary surface tension (S.T.) and thermo-capillary concentration convections

(Marangoni) were reduced. $In_{0.5}Ga_{0.5}Sb$ crystallization by VDS-process was enhanced.

IV. CONCLUSION

First time, the homogeneous and the entire detached crystals with composition and uniform structure was grown by a novel VDS-process. Dislocation density of ingots reduced to $10^3 cm^2$, the axial carrier mobility in n-type region.was $1.59x10^4$ $cm^2/V{\cdot}sec$, the axial resistivity decreased to $1.1x10^{-3}\Omega{\cdot}cm$. In p-type region, the highest hole mobility was ~$935cm^2/V.sec$. The preferred direction by XRD was (022). $In_{0.5}Ga_{0.5}Sb$ crystal fulfils substrates requirement of wavelength 2-8μm, Eg 0.16 to 0.68eV, and the lattice constants $6.096A^0$ to $6.479A^0$. The controlled growth, the thermo-gravitational convection into melt, and solute, heat and mass transport influence by gravity were reduced. Crystallization and the entire detached crystal growths by slow freezing from melt were superior. The crystalline quality, uniformity, smooth surface, reproducibility, and repetition were conformed.

REFERENCES

[1]. G. B. Stringfellow, Phys. Chem. Solids vol. 33, p. 665 (1972).
[2]. Qiang L, Jinwei W, Guofang H, Donghai Y, Weicai Z, Juncheng L; Vacuum 174 (2020) 109177
[3]. Zhengliang D, Jian H, Xiaolu C, Mengyi Y, Junhao Z, Yamei L; Inter metallics 112 (2019) 106528
[4]. D Li, C Lan, A Manikandan, S Yip, Z Zhou, X Liang, L Shu, Y Chueh, Nature Communications 10 (2019) 1664
[5]. Y Inatomi, M Arivanandhan, G Rajesh, Nirmal Kumar, Y Hayakawa NPJ Microgra 1(2019) 15011
[6]. Shan Y, Tan G, Yanxing L, Jiadong Z, Jing C, Litao KAibin H; Ceramics Intern 44 (2018) 22023
[7]. M. Streicher. V. Corregidor, N. Catarino, et.al Nucl Instru Metho Phy Rese B 371 (2016) 278–282
[8]. Yu J, Inatomi Y, Nirmal Kumar V, Hayakawa Y, Okano Y, Arivanandhan M, NPJ Microgr 5 (2015) 8
[9]. V. Strelov, B. Zakharo v, and A. Voloshin, Crystallographic Reports, 59(6) (2014) 781
[10]. Yu. Serebryakov, V. Prokhorov, I. Inve X-ray, Synch Neutron Techn 6(4) (2012) 604
[11]. J.P. Wöhrle, T. Jauss, A. Cröll, ICCGE19-2019 USA, Program Procee (2019) P-794
[12]. K. Wang, J. Peterson, J.Derby et.al. ICCGE 19-2019 USA, Prog Proc (2019) P-795
[13]. D.B. Gadkari, B.M. Arora, Material Chemistry and Physics 139 (2013) 375
[14]. D.B.Gadkari, Interna J. Sci Res Publ 4 (2014) 1
[15]. Dattatray Gadkari, Intern J Enginee Appl Sci (IJEAS) 2(4) (2015) 39
[16]. D. Gadkari, D. Maske, M. Deshpande, B Arora, Inten. J. Innov. Resea Sci. Eng 5(2) (2016) 2092
[17]. Dattatray Gadkari, J Electro Commu Engineering (IOSR-JECE) 12(4) IV (2017), 51-58
[18]. Dattatray Gadkari, J Electro Commu Engineering (IOSR-JECE) 13(3) (2018), 21-31
[19]. Dattatray Gadkari Int J Eng Res App 8(4) (2019) 01-19
[20]. D Maske, M Deshpande, D Gadkari, J Nano and Nano Electronis Physics; 12(2) (2020) 2012

Dr D B Gadkari, received B Sc (Physics) degree (1974) from Shivaji University, Kolhapur and M.Sc. degree in Physics from Bombay University (1976), and then University of Mumbai confirmed M Phil (1986) and Ph. D. under UGC-FIP (1998). He joined Mithibai College, Mumbai India (Nov-1976) as a Asst Prof, then HOD- Physics (2000-14), Asso prof (2006-2014), Vice-Principal (2010-2013) and Principal-I/C (2013-2014). He was Adjunct Research Guide-Faculty of Science: University of Mumbai (2014-2017), was at University of Mumbai- Board of Study Member in Physics (2005-2014), Faculty of Science Member (2005-2014); Board of Study Member in Bio-Physics (2010-2014). From June 1, 2017, Dr Gadkari is Freelance research and Consultant: Crystal Growth and Crystal Technology (Crystal Growth, Material Science, Solid State Physics and Physics of devices). He has been published 52 articles in referred journals and in the 32proceedings. The single crystal growth a new growth process - vertical directional solidification (VDS) has been developed successfully, and which shows the detached

phenomenon concept for Sb-based (III-V) quality bulk crystals in a terrestrial lab (on Earth). These crystals showed highest physical properties for crystals grown ever, while crystals are analogous to the crystal grown in microgravity. Member of professional International and National research journals. He has successfully completed Research projects (nine) sponsored by government of India and parent institute (SVKM). Indian patents in his name for the detached crystal growth by VDS in the terrestrial lab. This approach has opened a new area for high quality entire detached single crystal growth. He has received several kinds of awards/medals/certificates from academic societies such as Materials Chemistry and Physics, Indian Association of Crystal Growth, ASM International India Chapter, Shivaji University Kolhapur India, Several Research Institutes / Colleges within India and also from abroad.

D. B. Gadkari. "The homogeneous and entire detached In0.5Ga0.5Sb alloy crystals grown by the slow freezing using novel VDS-process." *International Journal of Engineering Research and Applications (IJERA*), vol.10 (05), 2020, pp 07-20.